ASSESSMENT OF MARS PATHFINDER LANDING SITE PREDICTIONS

M. P. Golombek[1], H. J. Moore[2], A. F. C. Haldemann[1], T. J. Parker[1], and J. T. Schofield[1]

[1]Jet Propulsion Laboratory
4800 Oak Grove Drive
California Institute of Technology
Pasadena, CA 91109

[2]U. S. Geological Survey
Astrogeology Team
Mail Stop 975
345 Middlefield Road
Menlo Park, CA 94025

Submitted March 13, 1998 to
Special Mars Pathfinder Issue of
Journal of Geophysical Research, Planets
Revised August 24, 1998

ABSTRACT

Remote sensing data at scales of kilometers and an Earth analog were used to accurately predict the characteristics of the Mars Pathfinder landing site at a scale of meters. The surface surrounding the Mars Pathfinder lander in Ares Vallis appears consistent with orbital interpretations that it would be a rocky plain composed of materials deposited by catastrophic floods. The surface and observed maximum clast size appears similar to predictions based on an analogous surface of the Ephrata Fan in the Channeled Scabland of Washington state. The elevation of the site measured by relatively small footprint delay-Doppler radar is within 100 m of that determined by two-way ranging and Doppler tracking of the spacecraft. The nearly equal elevations of the Mars Pathfinder and Viking Lander 1 sites allowed a prediction of the atmospheric conditions with altitude (pressure, temperature and winds) that were well within the entry, descent and landing design margins. High-resolution (~38 m/pixel) Viking Orbiter 1 images showed a sparsely cratered surface with small knobs with relatively low slopes, consistent with observations of these features from the lander. Measured rock abundance is within 10% of that expected from Viking orbiter thermal observations and models. The fractional area covered by large, potentially hazardous rocks observed is similar to that estimated from model rock distributions based on data from the Viking landing sites, Earth analog sites, and total rock abundance. The bulk and fine-component thermal inertias measured from orbit are similar to those calculated from the observed rock size-frequency distribution. A simple radar echo model based on the reflectivity of the soil (estimated from its bulk density), and the measured fraction of area covered by rocks was used to approximate the quasi-specular and diffuse components of the Earth-based radar echos. Color and albedo orbiter data was used to predict the relatively dust free or unweathered surface around the Pathfinder lander compared to the Viking landing sites. Comparisons with the experiences of selecting the Viking landing sites demonstrate the enormous benefit the Viking data and its analyses and models had on the successful predictions of the Pathfinder site. The Pathfinder experience demonstrates that in certain locations geologic processes observed in orbiter data can be used to infer surface characteristics where those processes dominate over other processes affecting the Martian surface layer.

INTRODUCTION

The successful landing of the Mars Pathfinder spacecraft and the collection of science and engineering data from the lander and rover allows the assessment of predictions made for the site based on Viking and Earth-based data. Prior to Pathfinder, direct observation of the Martian surface from the ground was limited to the two Viking landing sites, so the characteristics of other sites had to be inferred from remote sensing data at much coarser spatial resolutions.

Selection of the Mars Pathfinder landing site took place over a two and a half year period in which engineering constraints were identified, surface environments and safety considerations were developed (for the robust lander), and the potential science return at different sites was considered [*Golombek et al.,* 1997a]. Sites (100 km by 200 km target ellipses) were considered safe if they were below 0 km elevation (to provide enough atmosphere for parachute descent), were free of hazards in high-resolution (<50 m/pixel) Viking orbiter images (for a reasonably flat surface for final free fall and bounces), had acceptable reflectivity and roughness at radar wavelengths (for proper measurement of closing velocity with the radar altimeter during final descent), had relatively (compared to Mars average) high thermal inertia (for a relatively dust free and trafficable surface), moderate rock abundance (for scientific analyses), low red to violet ratio, and low albedo (for relatively dust free and/or unweathered rocks). The Ares Vallis site was selected because it appeared acceptably safe and offered the prospect of analyzing a variety of rock types deposited by catastrophic floods. Such a site would enable addressing first-order scientific questions like differentiation of the crust, the development of weathering products, and the nature of the early Martian environment and its subsequent evolution.

In selecting the Ares Vallis site using the remotely sensed data and the geologic setting, a number of predictions of the surface characteristics of the site were made [*Golombek et al.,* 1997a]. At the broadest level, we predicted that the Ares Vallis site would be safe for landing and roving with less dust and/or weathered surfaces and rocks than the two Viking lander sites. We also believed the surface would be a rocky plain, similar to catastrophic flood deposited surfaces on Earth, with the prospect of a variety of rock types available for study by the rover. This paper discusses both the overall predictions as well as the individual remote sensing observations used in evaluating the landing site and expectations of remote-sensing signatures based on the landed data.

The results indicate that the inferred properties of the surface derived from remote sensing data accurately predicted both the overall and specific characteristics of the surface.

GEOMORPHOLOGY AND GEOLOGICAL ANALOG

Many characteristics of the landing site are consistent with its being shaped by the Ares and Tiu catastrophic floods and their deposits [*Golombek et al.,* 1997b, this issue; *Smith et al.,* 1997]. These characteristics include: (1) a rocky surface with rounded to subrounded pebbles, cobbles and boulders that appear similar to those of depositional plains in terrestrial catastrophic floods (see later discussion), (2) large tabular rocks, many of which are perched, like those deposited by catastrophic floods, (3) imbricated rocks inclined in the direction of high discharge (such as in the Rock Garden, for location see Figures 7, 14 and 15 in *Golombek et al.* [this issue]), (4) streamlined hills in lander images, like the Twin Peaks (Figures 6, 7 and 14 in *Golombek et al.* [this issue]), in agreement with interpretations of them in Viking orbiter images of the region, and (5) a broad, gentle ridge trending northeast from Twin Peaks [*Golombek et al.,* 1997b]. This broad, gentle ridge, which is the rise to the north of the lander, is aligned in the downstream direction from the Tiu Vallis floods, and may be a debris tail deposited in the wake of the Twin Peaks (Figure 6 in *Golombek et al.* [this issue]). Troughs visible throughout the scene may be primary features produced by the flood or they may be a result of late stage drainage of water that preferentially carried away the fines leaving an armored and rocky surface.

During the selection of the landing site, the Channeled Scabland in Washington state was studied as an analog to Ares Vallis [*Golombek et al.,* 1995, 1997a]. In particular, the 40 km long Ephrata Fan, deposited where channelized water flowing down the Grand Coulee filled the Quincy Basin, was compared with the depositional area in Chryse Planitia, where the landing site is located (see Figure 5 in *Golombek et al.* [this issue]). The gradient in clast size with distance from the mouth of the channel on the Ephrata Fan [*Baker,* 1972] suggests that the largest clasts carried by the catastrophic floods (estimated at 10 m intermediate dimension, [*Komatsu and Baker,* 1997]) would have been deposited about 100 km south of the landing site where the channel debouches into Chryse Planitia. Thus it was anticipated that the landing site would have moderate rock abundances [*Rice and Edgett,* 1997; *Edgett and Christensen,* 1997], with rocks considerably

smaller than 10 m [*Golombek and Rapp,* 1997], and that it would be relatively safe for landing and roving [*Golombek et al.,* 1997a]. The overall geology, geomorphology, and appearance of the landing site is similar to those of the depositional Ephrata Fan (Figure 1), as interpreted from orbital images prior to landing [*Golombek et al.,* 1997a] and the abundance and size of pebbles, cobbles and boulders are consistent with the expected general decrease in clast size from the mouth of the channel [*Baker,* 1972, *Golombek et al.,* 1997a]. Images acquired by Pathfinder also imply that a variety of rock types may be present at the landing site [*Golombek et al.,* this issue] as would be expected in material eroded and subsequently deposited in a catastrophic flood that flowed across heterogeneous materials.

In general the surface at the Pathfinder landing site appears to have changed little since it formed billions of years ago [*Golombek et al.,* this issue; *Ward et al.,* this issue], with the exception that eolian activity may have deflated or exhumed the surface by 5-7 cm, deposited wind tails of fine dust, collected sand into dunes, and eroded ventifacts (fluted and grooved rocks) [*Greeley et al.,* this issue]. Impact cratering has also modified the site, but its effect appears to be limited to deposition of small, angular dark rocks (ejecta) [*Smith et al.,* 1997]. The lack of extensive post-flood erosion and/or deposition of the site is probably why it appears similar to the Ephrata Fan, which has not been extensively modified since the latest flood (less than 1 m loess and volcanic ash have accumulated since the flood about 12,000 years ago [e.g., *Baker,* 1972; *Rice and Edgett,* 1997]).

ELEVATION

The elevation of the Pathfinder landing site was assessed prior to landing as a critical input for entry, descent and landing analysis and design. The primary data were obtained from three delay-Doppler radar tracks that provided ranging across the designated landing ellipse [*Haldemann et al.,* 1997]. The average values of the radar ranging for all three tracks within the ellipse boundaries are reported as planetary radius in Table 1. The radar observations were compared with both the 6.1 mbar Mars geoid, based on the 4th order and degree gravity field [e.g., *U.S. Geological Survey,* 1993], and the Mars 50c geoid, based on the 50th degree and order gravity field [*Konopliv and Sjogren,* 1995], as well as with elevation information for Viking Lander 1

[*Yoder and Standish,* 1997]. The difference in elevation with Viking 1 was critical for deriving the atmospheric profile for planning key events during entry, descent and landing. After landing, once the location of the lander was determined by two-way tracking [*Folkner et al.*, 1997], its exact elevation was compared with the values of radar ranging data for the 6 radar resolution cells (10 km by 150 km) that contain the lander [*Haldemann et al.,* 1997].

It was predicted prior to landing that the average elevation of the center of the site would be about the same elevation as Viking Lander 1 relative to the 6.1 mbar geoid [*Haldemann et al.,* 1997] and on Viking tracking results [*Yoder and Standish,* 1997]. The Doppler tracking and two-way ranging estimate for the elevation of the spacecraft is 3389.72±0.03 km relative to the center of mass of the planet [*Folkner et al.,* 1997]. The elevation of the lander with respect to the 6.1 mbar geoid is -1.66 and only 60 m lower than the Viking 1 lander; results for the Mars 50c geoid [*Konopliv and Sjogren,* 1995] indicates Pathfinder is 110 m lower than Viking Lander 1. The elevation of the lander is also within 100 m of the elevations derived from the delay-Doppler radar tracks that contain it, which represents remarkable agreement within the uncertainties of the measurements. Note that these result vary slightly from those reported earlier in *Golombek et al.* [1997b] owing to a more precise selection of the geoid at the actual lander location that takes into account the cartographic/inertial frame offset [*Golombek et al.,* this issue].

ATMOSPHERIC CONDITIONS

The atmospheric conditions used to design and model entry, descent and landing [*Spencer and Braun*, 1996; *Braun et al.,* 1997] were based on a combination of Viking data, Earth-based observations, and general circulation models. As the Viking 1 and Pathfinder landing sites are at similar latitudes and altitudes (based on the radar data), Viking 1 surface temperatures, pressures and winds at the Pathfinder landing season and local solar time were assumed. The model assumed a surface elevation of -1.593 km relative to the 6.1 mbar datum. The predicted vertical atmospheric structure was also influenced by Earth-based microwave observations, modified near the surface for time of day effects. Considerable margin was provided to accommodate uncertainties in vertical temperature structure. In the absence of suitable Mars data, vertical wind shear in the lower 10 km of the atmosphere was scaled from terrestrial wind shear data sets.

After landing (Table 2), surface pressures and winds (5-10 m/sec) were found to be very similar to expectations (see low level winds in *Golombek et al.*, [1997a]), although temperatures were approximately 10 K warmer (measured on sol 3 at 03:00 local solar time [*Schofield.* et al., 1997]). Higher temperatures are consistent with the lower surface albedo (0.24) and greater surface thermal inertia (10.4) of the Pathfinder landing site relative to the Viking Lander 1 site (albedo ~0.29, thermal inertia ~8.4 x 10^{-3} cgs units, see later discussion) [*Palluconi and Kieffer,* 1981]. Pathfinder's atmospheric profiles during entry are based on the accelerometer measurements which provide density directly. Pressure is derived from density versus height using the hydrostatic equation, and temperature comes from the ideal gas law given pressure and density. The temperature profile below 50 km was roughly 20 K warmer than the model, so the pressure scale height is larger than assumed in the model. As a result, observed densities were 5% lower near the surface and a factor of 2 higher at 50 km, though still well within the entry, descent and landing design margins.

HIGH-RESOLUTION IMAGING DATA

The gently undulating surface seen over large distances around the lander is consistent with a surface relatively free of hazardous slopes that was predicted with high-resolution (38 m/pixel) images of the landing site (Table 3). Only 1.2% of the surface was measured to be covered by craters in Viking orbiter images [*Golombek et al.*, 1997a] and 3 small craters are visible from the lander (1.5 km, 0.15 km and 0.14 km diameters) [*Golombek et al.*, this issue]. Given the size-frequency distribution of craters measured at the site [*Parker and Rice,* 1997], there is a 40% probability of landing at a location within view of three such craters, implying that the lander is actually in a more heavily cratered region of the ellipse than average.

Small hills and mesas measured in orbiter images cover 0.7% of the landing ellipse surface and photoclinometry measurements indicated generally low slopes (average slopes of 10°, maximum slopes of 25°) [*Golombek et al.*, 1997a]. Slopes of north and south Twin Peaks measured in lander images are consistent with these estimates (14°-27°). Larger hills such as Far (Figure 1), Southeast and North Knobs (see Figure 6, 8 and 9 in *Golombek et al.*, [this issue]) have steeper slopes (>30°), consistent with their steeper slopes in high-resolution Viking

topographic maps [*Howington-Kraus et al.*, 1995]. Given the size-frequency distribution of knobs measured at the site [*Golombek et al.*, 1997a], there is only a 10% probability of landing at a location within view of four knobs, implying that the lander is in a region of the ellipse with many more knobs than average. Preliminary quantitative measurements of meter-scale root-mean-square slopes have been calculated from digital terrain maps derived from stereo images acquired by the lander camera [*Smith et al.*, 1997, Plate 4]. These results (4°) appear to be roughly consistent with root-mean-square slopes near 5° for the smallest footprint [*Haldemann et al.*, 1997] and slightly larger slopes for larger footprint radar measurements (Table 3).

ROCK ABUNDANCE

The rock size-frequency distribution was determined from the measurement of rock apparent diameters using the Marsmap virtual reality data visualization program [*Stoker et al.*, this issue]. Rock diameters perpendicular to a radial from the local lander coordinate center were measured from the lander imagery. Note that the apparent diameter is some combination of the length and width of the rock depending on its aspect ratio and orientation with respect to the imager. In this analysis, rocks are assumed to have circular bases to calculate areal coverage. Preliminary comparisons of measurements of each axis indicate the assumption of circular bases has little effect on these results (<20%); uncertainty in the diameter measurements is 1 cm. The cumulative fractional area within an annulus from 3 m to 6 m radius centered in the lander local coordinate frame covered by rocks with diameters greater than 3 cm is 16.1%. Within the annulus the rock cumulative fractional area coverage in the eastern third is only 10.2%, while for the southwestern third (Rock Garden) it is 24.6%. Rock heights were also measured as the maximum difference between the top of the rock and the ground surrounding the rock. Plots of cumulative fractional area covered by rocks larger than a given diameter or height are plotted in Figures 2 and 3 for the entire annulus. The distribution of large rocks appears skewed due to the presence of Yogi (see Figure 15 in *Golombek et al.*, [this issue]) within the annulus (a large rock within a small counting area). As a result, an attempt was made to measure the size of large rocks in the far field to better constrain the size-frequency distribution of these potentially hazardous rocks. Rocks beyond the 3 to 6 m annulus were measured from vertical stereo comparisons of the pre- and post-

mast deployment panoramas. All rocks with one dimension greater than 20 pixels and visible in both panoramas were measured. This produced a set of 56 far-field rocks that were binned according to their size. For example a 2 m rock would be 20 pixels in size if it were within 200 m of the lander (IMP pixel resolution about 1 mrad). Thus, a 2 m rock is only included if it is nearer than 200 m, and the area considered for 2 m rocks is the 200 m radius circle around the lander (Figure 2).

The rock-strewn surface at Ares is reasonably consistent with expectations prior to landing (Table 3). Expectations were about 20% (18% for the pixel containing the lander) as indicated by rock abundances from Viking orbiter Infrared Thermal Mapper (IRTM) observations [*Christensen,* 1986b, *Edgett and Christensen,* 1997], which is similar to the 16% measured at the site. *Christensen* [1982, 1986b] assumed an effective thermal inertia of 30 (10^{-3} cgs units or 10^{-3} calories cm^{-2} $s^{-0.5}$ K^{-1})) for the rock population which corresponds to spherical rocks ~0.10 m in diameter [*Christensen,* 1986b, *Christensen and Moore,* 1992]; below we obtain a modestly different effective thermal inertia for the rock population. A rocky surface was also suggested by the nearby Viking 1 site which has similar rock coverage [*Moore and Keller,* 1990, 1991], but a somewhat lower rock abundance (about 15%) [*Christensen* , 1986b].

Model rock distribution estimates for the Ares Vallis site derived from those measured at the Viking landing sites, Earth analog sites, and from IRTM estimates are similar to those observed at the site [*Golombek and Rapp,* 1997]. These models indicated that about 0.7-3% of the area would be covered by potentially hazardous rocks that are greater than 1 m in diameter or 0.5 m high [*Golombek and Rapp,* 1997], which is close to that measured around the lander (Figures 2 and 3). The far field estimates of large rocks are consistent with the predicted rapid drop in fractional area covered by these potentially hazardous boulders. Using the far field rocks (and the commensurably larger counting area) combined with Yogi in the near field suggests that rocks higher than 0.5 m cover an area less than 1% (0.5%) and rocks greater than 1 m in diameter cover and area considerably less than 1% (0.2%).

THERMAL INERTIA

We have estimated an effective thermal inertia near 40 (10^{-3} cgs units or 10^{-3} calories cm^{-2} $s^{-0.5}$ K^{-1}) for the entire rock population (compared with 30 assumed for the IRTM analysis above) by summing the products of the thermal inertias and areas for each rock and dividing by the total area covered by the rocks (Table 3, Figure 2). In the estimate based on the model of *Jakosky* [1986], rocks greater than 0.26 m in diameter have inertias near 50 (10^{-3} cgs units) and smaller ones vary as the 0.75 power of their diameter; 0.03 m rocks have inertias near 10. Using a bulk thermal inertia of 10.4 [*Palluconi and Kieffer,* 1981] for the landing site and a graphical representation of Kieffer's model [*Kieffer et al.,* 1977], we obtain a fine-component inertia near 8.4 which agrees with the fine-component inertia of 8.7 (in 10^{-3} cgs units) estimated from thermal observations from orbit by the IRTM [*Christensen,* 1982, 1986a]. Fine component inertias of this magnitude are consistent with the presence of cohesionless, well-sorted, sand-size materials [e.g. *Presley and Christensen*, 1997a,b], poorly-sorted granular mixtures [*Jakosky* 1986], and cemented soil-like deposits [*Jakosky and Christensen*, 1986]. The presence of sand-size material, poorly-sorted granular mixtures, and cemented soil-like deposits have been inferred from Sojourner and Mars Pathfinder observations [*Moore et al.,* this issue; *Greeley et al.,* this issue] and these materials present no difficulties to landing or roving nor would materials inferred from the smaller inertias in other models [*Haberle and Jakosky*, 1991; *Hayashi et al.*, 1995].

RADAR REFLECTIVITY

The validity of interpretations of radar echoes prior to landing are supported by a simple radar echo model [*Evans and Hagfors,* 1964], an estimate of the reflectivity of the soil, and the fraction of area covered by rocks. The model relates the total cross-section of the polarized echo (σ_{oc}) with the quasi-specular (σ^{Q}_{oc}) and the diffuse (σ^{D}_{oc}) components: $\sigma_{oc} = \sigma^{Q}_{oc} + \sigma^{D}_{oc}$. The quasi-specular component (σ^{Q}_{oc}) is related to the normal reflectivity (ρ_o), the root-mean-square slope in radians (Θ_r), a number near unity, and the area (X) producing the quasi-specular echo. The diffuse component is related to the reflectivity of the wavelength scatters (ρ_r), the directivity, and the fraction of area of scatterers producing the diffuse echo: $\sigma_{oc} = \rho_o (1 + n \Theta_r^2) X + \rho_r\ g (1-X)$, where $\rho_o = 0.06$, $\Theta_r = 4.8°$, $X = 0.839$, $\rho_r = 0.23$, and $g=2$. In the calculations, the soil

produces the quasi-specular echo and the rocks, which generally have knobby surfaces, produce the diffuse echo. For the soil, the reflectivity is estimated to be near 0.04-0.06 in a two-step process. First, the soil is assumed to be similar to lunar soil simulant [*Mitchell et al.*, 1972] so that its bulk density can be taken as 1.285-1.518 g/cm^3 because its friction angle is near 34.3°-36.6° [*Moore et al.*, this issue; *Rover Team*, 1997]. Second, the reflectivity is estimated from a relation between bulk density and normal reflectivity [*Olhoeft and Strangway*, 1975]. In the model, the quasi-specular cross-section is reduced to 0.034-0.050 by the fraction of area covered by the reflector (0.839) and enhanced (1.007) by the root-mean-square slope term (taken as 4.8°). This is comparable to the reflectivities of 0.06±0.02 reported from the 3.5-cm delay-Doppler observations (for small root-mean-square-slopes, reflectivities and quasi-specular cross-sections are nearly equal), which are modestly larger than the 0.045 reported for the continuous-wave observations (Table 3). For the diffuse echo, rocks cover 16.1% of the surface and are assumed to have a reflectivity and directivity appropriate for rocks (0.23 and 2, respectively [*Thompson and Moore*, 1989]). With these values, the model yields a polarized diffuse echo cross section of 0.07 - a value close to the 0.055 reported for 3.5-cm wavelength observations [*Haldemann et al.*, 1997]. At 12.5-cm wavelength, similar rock populations at Ares and the Viking 1 site are expected because the diffuse echoes are comparable [*Harmon*, 1997], but the large quasi-specular reflectivities (~0.12-0.13) suggests bulk densities greater than 2.2 g/cm^3. One possible explanation is that bulk densities of soils (perhaps like Scooby Doo) at depth are larger than those at the surface. In any event, the successful landing and roving at Ares is consistent with the pre-landing site appraisal of the radar echoes.

COLOR AND ALBEDO

Appraisal of orbiter color and albedo data prior to landing suggested that surfaces of materials at Ares Vallis would be relatively dust-free and unweathered [*Golombek et al.*, 1997a] when compared with the materials at the Viking landing sites, where many of the rocks were apparently coated with bright red dust and/or varnish [*Guinness et al.*, 1987, 1997]. This suggestion may be manifested by a greater abundance of relatively dark-gray rocks [*McSween et al.*, this issue] and dark-gray surfaces of soils [*Smith et al.*, 1997] and smaller areas of drifts at the

Pathfinder site than at the Viking sites. There are no quantitative assessments of the relations of color data at the three landing sites, but it is our impression that dark-gray rocks and dark-gray soil-like deposits are more abundant at the Pathfinder site than at the Viking sites.

DISCUSSION

There are important differences as well as many parallels in the Pathfinder and Viking landing site selection and certification processes. Among the differences are: (1) knowledge of the atmosphere for entry, descent, and landing, (2) method of landing (e.g., legs versus airbags), (3) available images and sophistication of analyses of them, (4) completeness and sophistication of radar-echo data analyses, (5) completeness and sophistication of analyses of thermal data, (6) previous experience on the surface of Mars, (7) a "learn as you go" philosophy in which changes were made during the mission, (8) scientific goals and (9) selection of a site for which there appeared to be an obvious Earth analog. Among the parallels are a comparable list of data and acceptable parameters that were needed for successful landings [*Masursky and Crabill,* 1981; *Golombek et al.,* 1997a].

As it turned out for Viking 1, the actual measurement of atmospheric properties were well within the engineering models and design tolerances [*Masursky and Crabill,* 1976a, 1981] and the second landing profited from the first. For the Viking landers, 22-cm high rocks were considered hazardous; Pathfinder sought rocks. Maps of the initial Viking Chryse site (centered at 19.5°N, 34.0°W), which is just west of the Pathfinder site, were prepared using Mariner 9 images [*Masursky and Strobell,* 1976, see p. 24-27] that included atmospheric haze from the dissipating Great Dust Storm of 1971. Upon arrival, Viking Orbiter 1 acquired images of the site through clear skies that were astonishing because they revealed an eroded surface in the etched terrain that was not visible in the Mariner 9 images and many felt that the surface would be rocky (partly by analogy with the Channeled Scabland of Washington). This situation caused the rejection of the site and the search for a more amenable surface. Arecibo radar observations at 12.6-cm [*Tyler et al.,* 1976] were important considerations for Lander 1 and held as much weight as the images [*Masursky and Crabill,* 1976a, 1981]. Unlike Pathfinder, Goldstone echoes were weak, suggesting a very rocky or rough surface, and diffuse echoes at 3.6- and 12.6-cm were not

available or assessed. After selecting an alternative site while in orbit, Lander 1 descended to a surface that appeared to have soil-like materials at the surface, root-mean-square slopes like some lunar maria and Surveyor sites on the Moon, and a reflection coefficient that was Mars average.

Viking Lander 2 benefited from newly acquired data on the atmosphere and successful landing of Lander 1 [*Masursky and Crabill,* 1976b]. Science dictated sending Lander 2 to the northern latitudes where there were larger amounts of water vapor in the atmosphere and a greater likelihood of life [*Masursky and Crabill,* 1976b, 1981]. Radar data were not available for the northern latitudes, so that thermal observations as well as images figured strongly in interpretations of the Lander 2 site. Sophisticated analyses of fine-component thermal inertias and rock abundances were not available, but it was postulated that the Lander 2 site could be either rocky like the Lander 1 site or sandy; a similar ambiguity still exists [see *Golombek et al.,* 1997a]. Interpretations of the images varied: (1) some thought the surface would be sandy, (2) others rocky, and (3) still others, a fine-grained eolian mantle.

The data list (parameter and source) developed for Viking resembles that of Pathfinder [*Masursky and Crabill,* 1981; *Golombek et al.,* 1997a]. The "surface" list includes: (1) altitude (Earth-based radar and stereo-imaging, <4.25 km), (2) temperature (infrared thermal mapper), (3) geology (visual impressions), (4) slopes (Earth-based radar and images, <19°), (5) protuberances (visual impressions, <22 cm), (6) density, grain size, and cohesion (Earth-based radar and visual impressions, 1.2-1.9 g/cm^3) , and (7) radar reflectivity (Earth-base radar, >1% for altimeter). The "atmospheric" list includes: (1) density and temperature as function of altitude (microwave atmospheric water vapor detector and infrared thermal mapper), (2) composition (<15-20% argon), (3) dust storms (images), and (3) winds (cloud motion and albedo changes).

Importantly, Viking Landers 1 and 2 and Pathfinder landed successfully. Viking did not have the benefit of previous experience like Pathfinder. Clearly, Pathfinder profited from (1) atmospheric data, (2) images, (3) complete thermal observations, and (4) orbital color data supplied by Viking during entry and from orbit. The use of radar echoes for site selection and certification Mars was pioneered by the Viking Project [*Tyler et al.,* 1976; see also, *Simpson et al.,* 1978a,b]. Likewise, the Viking landers supplied data on (1) albedos and colors of soils and rocks that guided the imaging and rover traverse planning strategy for sampling rocks and (2) physical-

mechanical properties of the surface materials and rock populations that were used during the design, testing, and site selection phases.

CONCLUSIONS

Using the data acquired by Viking and sophisticated analysis and modeling of the data allowed us to predict the important characteristics of the Pathfinder site for safe landing and roving at a scale of meters even though the remote sensing data are at scales of kilometers to tens of kilometers. The prediction that the site would be a plain composed of materials deposited by a catastrophic flood is consistent with that found at the surface and implies that some geologic processes observed in orbiter data can be used to infer surface characteristics where those processes dominate over other processes affecting the Martian surface layer [e.g., *Christensen and Moore,* 1992]. The fact that the site appears to have changed little since it formed billions of years ago also likely contributed to the retention of its primary depositional and morphological attributes. For other areas on Mars, dust and sediment transport may obscure primary geologic features of surfaces making them more difficult to predict from remotely sensed data. Close up rover and lander images suggest that a variety of rock types and materials (a "grab bag" sample) were deposited by the flood.

ACKNOWLEDGMENTS

Work described in this paper was carried out by the Mars Pathfinder Project at the Jet Propulsion Laboratory, California Institute of Technology under contract with the National Aeronautics and Space Administration. We thank Nathan Bridges for measuring far field rocks, estimating the probability of seeing knobs and crater rims from the lander, and for ideas and discussions. Thanks to K. Edgett and E. Guiness for comments on an earlier version of the manuscript. We are deeply indebted to the engineers on the Pathfinder team for offering us the opportunity to test our predictions with data from the surface of Mars.

REFERENCES

Baker, V. R., Paleohydrology and sedimentology of Lake Missoula flooding in eastern Washington, *Geol. Soc. America Spec. Pap. 144,* 73 p., 1972.

Braun, R. D., D. A. Spencer, P. H. Kallemeyn, and R. M. Vaughan, Mars Pathfinder atmospheric entry navigation operations, *American Institute of Aeronautics and Astronautics paper 97-3663*, at AIAA GNC, AFM, and MST Conference, New Orleans, Aug. 11-13, 1997.

Christensen, P. R., Martian dust mantling and surface composition: Interpretation of thermophysical properties, *J. Geophys. Res., 87*, 9985-9998, 1982.

Christensen, P. R., Regional dust deposits on Mars: Physical properties, age, and history, *J. Geophys. Res., 91*, 3533-3545, 1986a.

Christensen, P. R., The spatial distribution of rocks on Mars, *Icarus, 68*, 217-238, 1986b.

Christensen, P. R. and H. J. Moore, The martian surface layer, in MARS edited by H. H. Kieffer, B. M. Jakosky, C. W. Snyder, and M. S. Matthews, University of Arizona Press, 686-727, 1992.

Edgett, K. S., and P. R. Christensen, Rocks and aeolian features in the Mars Pathfinder landing site region: Viking infrared thermal mapper observations, *J. Geophys. Res, 102,* 4107-4116, 1997.

Evans, J. V., and T. Hagfors, On the interpretation of radar reflections from the Moon, *Icarus, 3,* 151-160, 1964.

Folkner, W. M., C. F. Yoder, D. N. Yuan, E. M. Standish, and R. A. Preston, Interior structure and seasonal mass redistribution of Mars from radio tracking of Mars Pathfinder, *Science, 278*, 1749-1752, 1997.

Golombek, M. P., K. S. Edgett, and J. W. Rice Jr., eds., *Mars Pathfinder Landing Site Workshop II: Characteristics of the Ares Vallis Region and Field Trips in the Channeled Scabland, Washington*, Lunar and Planetary Institute Technical Report 95-01, 1995, Part 1, 63 pp; and Part 2, 47 pp., 1995.

Golombek, M., and Rapp, D., Size-frequency distributions of rocks on Mars and Earth analog sites: Implications for future landed missions, *J. Geophy. Res., 102,* 4117-4129, 1997.

Golombek, M. P., R. A. Cook, H. J. Moore, and T. J. Parker, Selection of the Mars Pathfinder landing site, *J. Geophy. Res., 102*, 3967-3988, 1997a.

Golombek, M. P., R. A. Cook, T. Economou, W. M. Folkner, A. F. C. Haldemann, P. H. Kallemeyn, J. M. Knudsen, R. M. Manning, H. J. Moore, T. J. Parker, R. Rieder, J. T. Schofield, P. H. Smith, and R. M. Vaughan, Overview of the Mars Pathfinder Mission and assessment of landing site predictions, *Science, 278*, 1743-1748, 1997b.

Golombek, M. P., et al., Overview of the Mars Pathfinder mission: launch through landing, surface operations, data sets, and science results, *J. Geophys. Res.*, this issue.

Greeley, R., M. Kraft, G. Wilson, N. Bridges, K. Herkenhoff, R. O. Kuzmin, M. Malin, R. Sullivan, and W. Ward, Aeolian features and processes at the Mars Pathfinder landing site, *J. Geophys. Res.*, this issue.

Guinness, E. A., R. E. Arvidson, M. A. Dale-Bannister, R. B. Singer, and E. A. Bruckenthal, On the spectral reflectance properties of materials exposed at the Viking landing sites, *J. Geophys. Res., 92*, E575-E587, 1987.

Guinness, E. A., R. E. Arvidson, I. H. D. Clark, and M. K. Shepard, Optical scattering properties of terrestrial varnished basalts compared with rocks and soils at the Viking Lander sites, *J. Geophys. Res., 102*, 28,687-28,703, 1997.

Haberle, R. M. and B. M. Jakosky, Atmospheric effects on the remote determination of thermal inertia on Mars, *Icarus, 90*, 187-204, 1991.

Haldemann, A. F. C., D. L. Mitchell, R. A. Jurgens, M. A. Slade, and D. O. Muhleman, Mars Pathfinder landing site assessment with Goldstone delay Doppler and CW radar experiments *J. Geophys. Res., 102*, 4097-4106, 1997.

Harmon, J. K., A radar study of the Chryse Region, Mars, *J. Geophys. Res., 102*, 4081-4095, 1997.

Hayashi, J. N., B. M. Jakosky, and R. M. Haberle, Atmospheric effects on the mapping of Martian thermal inertia and thermally derived albedo: *J. Geophys. Res., 100*, 5277-5284, 1995.

Howington-Kraus, E., R. L. Kirk, B. Redding, and L. A. Soderblom, High-resolution topographic map of the Ares Tiu landing site from Viking Orbiter data, p. 38, in

Golombek, M. P., K. S. Edgett, and J. W. Rice Jr., eds., *Mars Pathfinder Landing Site Workshop II: Characteristics of the Ares Vallis Region and Field Trips in the Channeled Scabland, Washington*, Lunar and Planetary Institute Technical Report 95-01, 1995, Part 2, 47 pp., 1995.

Jakosky, B. M., On the thermal properties of Martian fines, *Icarus, 66*, 117-124, 1986.

Jakosky, B. M., and P. R. Christensen, Global duricrust on Mars: Analysis of remote sensing data, *J. Geophys. Res., 91*, 3547-3559, 1986.

Kieffer, H. H., T. Z. Martin, A. R. Peterfreund, B. M. Jakosky, E. D. Miner, and F. D. Palluconi, Thermal and albedo mapping of Mars during the Viking Primary Mission, *J. Geophys. Res., 82*, 4249-4291, 1977.

Komatsu, G., and V. R. Baker, Paleohydrology and flood geomorphology of a martian outflow channel: Ares Vallis, *J. Geophys. Res., 102*, 4151-4160, 1997.

Konopliv, A. S., and W. L. Sjogren, The JPL Mars gravity field, Mars 50c, based on Viking and Mariner 9 Doppler tracking data, *JPL Publication 95-5*, 73 pp., Feb. 1995.

Masursky, H., and M. H. Strobell, Geologic maps and terrain analysis data for Viking Mars '75 landing sites considered in December, 1972, *U. S. Geological Survey Interagency Report*, Astrogeology 59, Open-File Report 76-431, 73p., 1976.

Masursky, H., and N. L. Crabill, The Viking landing sites: Selection and certification, *Science, 193*, 809-812, 1976a.

Masursky, H., and N. L. Crabill, Search for the Viking 2 landing site, *Science, 194*, 62-68, 1976b.

Masursky, H., and N. L. Crabill, Viking site selection and certification, *NASA SP-429*, 34pp., 1981.

McSween, H. Y., S. L. Murchie, J. A. Crisp, N. T. Bridges, R. C. Anderson, J. F. Bell, D. T. Britt, J. Bruckner, G. Dreibus, T. Economou, A. Ghosh, M. P. Golombek, J. P. Greenwood, J. R. Johnson, H. J. Moore, R. V. Morris, T. J. Parker, R. Rieder, R. Singer, and H. Wanke, Chemical, multispectral, and textural constraints on the composition and origin of rocks at the Mars Pathfinder landing site, *J. Geophys. Res.*, this issue.

Mitchell, J. K., W. N. Houston, R. F. Scott, N. C. Costes, W. D. Carrier III, and L. G. Bromwell, Mechanical properties of lunar soils: Density, porosity, cohesion, and angle of internal friction, *Proc. Third Lunar Science Conf., Sup. 3, Geochim et Cosmochim Acta*, 3, 3235, 1972.

Moore, H. J. and J. M. Keller, Surface material maps of the Viking landing sites on Mars (abs.), *Reports of Planetary Geology and Geophysics Program - 1989*, NASA Tech. Mem. 4210, 533-535, 1990.

Moore, H. J. and Keller, J. M., Surface material maps of the Viking landing sites on Mars (abs.), in *Reports of Planetary Geology and Geophysics Program - 1990*, NASA Tech. Mem. 4300, 160-162, 1991.

Moore, H., D. Bickler, J. Crisp, H. Eisen, J. Gensler, A. Haldemann, J. R. Matijevic, F. Pavlics, and L. Reid, Soil-like deposits observed by Sojourner, the Pathfinder rover, *J. Geophy. Res.*, this issue.

Olhoeft, G. R., and D. W. Strangway, Dielectrical properties of the first 100 meters of the Moon, *Earth Planet. Sci. Letts., 24*, 394-404, 1975.

Palluconi, F. D., and H. H. Kieffer, Thermal inertia mapping from 60°S to 60°N, *Icarus, 45*, 415-426, 1981.

Parker, T. J., and J. W. Rice, Sedimentary geomorphology of the Mars Pathfinder landing site, *J. Geophy. Res., 102*, 25,641-25,656, 1997.

Presley, M. A., and P. R. Christensen, Thermal conductivity measurements of particulate materials, 2, results, *J. Geophy. Res., 102*, 6551-6566, 1997a.

Presley, M. A., and P. R. Christensen, The effect of bulk density and particle size sorting on thermal conductivity of particulate materials under Martian atmospheric pressures, *J. Geophy. Res., 102*, 9221-9229, 1997b.

Rice, J. W., Jr., and K. S. Edgett, Catastrophic flood sediments in Chryse Basin, Mars, and Quincy Basin, Washington: Application of sandar facies model, *J. Geophy. Res., 102*, 4185-4200, 1997.

Rover Team, Characterization of the Martian surface deposits by the Mars Pathfinder rover, Sojourner, *Science, 278*, 1765-1768, 1997.

Schofield, J. T., J. R. Barnes, D. Crisp, R. M. Haberle, S. Larsen, J. A. Magalhaes, J. R. Murphy, A. Seiff, and G. Wilson, The Mars Pathfinder atmospheric structure investigation/meteorology (ASI/MET) experiment, *Science, 278*, 1752-1758, 1997.

Smith, P. H., J. F. Bell, N. T. Bridges, D. T. Britt, L. Gaddis, R. Greeley, H. U. Keller, K. E. Herkenhoff, R. Jaumann, J. R. Johnson, R. L. Kirk, M. Lemmon, J. N. Maki, M. C. Malin, S. L. Murchie, J. Oberst, T. J. Parker, R. J. Reid, R. Sablotny, L. A. Soderblom, C. Stoker, R. Sullivan, N. Thomas, M. G. Tomasko, W. Ward, and E. Wegryn, Results from the Mars Pathfinder camera, *Science*, *278*, 1758-1765, 1997.

Simpson, R. A., G. L. Tyler, and D. B. Campbell, Arecibo radar observations of Martian surface characteristics near the equator, *Icarus*, 33, 102-115, 1978a.

Simpson, R. A., G. L. Tyler, and D. B. Campbell, Arecibo radar observations of Martian surface characteristics in the northern hemisphere, *Icarus*, 36, 153-173, 1978b.

Spencer, D.A., and R.D. Braun, Mars Pathfinder atmospheric entry: trajectory design and dispersion analysis, *J. Spacecraft Rockets*, *33*, 5, 670-676, 1996.

Stoker, C. R., E. Zbinden, T. T. Blackmon, B. Kanefsky, J. Hagen, P. Henning, C. Neveu, D. Rasmussen, K. Schwehr, and M, Sims, Analyzing Pathfinder data using virtual reality and super-resolved imaging, *J. Geophy. Res.*, this issue.

Thompson, T. W., and H. J. Moore, A model for Mars depolarized radar echoes from Mars: *Proc. 19th Lunar Planet. Sci. Conf.*, 409-422, 1989.

Tyler, G. L., D. B. Campbell, G. S. Downs, R. R. Green, and H. J. Moore, Radar characteristics of the Viking landing sites, *Science, 193*, 812-815, 1976.

U.S. Geological Survey, Mission to Mars: Digital Topographic Map, Volume 7, Global Topography, Compact Disc: USA_NASA_PDS_VO_2007, Version 2, 1993-01-21, 1993.

Yoder, C. F., and E. M. Standish, Martian moment of inertia from Viking lander range data, *J. Geophys. Res. 102*, 4065, 1997.

Ward, A. W., L. R. Gaddis, R. L. Kirk, L. A. Soderblom, K. L. Tanaka, M. P. Golombek, T. J. Parker, R. Greeley, and R. O. Kuzmin, General geology and geomorphology of the Mars Pathfinder landing site, *J. Geophys. Res.*, this issue.

Table 1. Landing Site Elevations

Location Elevation Data	Planetary Radius (km)	Elevation Relative to Geoid (Geoid Elevation): 6.1 mbar Geoid (km)	 Mars 50c Geoid (km)
Viking Lander 1 Site			
48.22°W, 22.48°N		(3390.92)	(3390.38)
USGS DTM	3389.35	-1.57	-1.03
Tracking	3389.32±0.02	-1.60±0.02	-1.06±0.02
Ares Vallis Target Ellipse			
33.10°W, 19.43°N		(3391.25)	(3390.79)
USGS DTM	3389.19	-2.06	-1.60
Radar	3389.66±0.03	-1.59±0.03	-1.13±0.03
Pathfinder Landing Site			
33.52°W, 19.28°N		(3391.38)	(3390.88)
USGS DTM	3389.34	-2.04	-1.55
Radar	3389.63±0.04	-1.75±0.04	-1.25±0.04
Tracking	3389.72±0.03	-1.66±0.03	-1.17±0.03

USGS DTM values and geoid values for the Viking 1 and Pathfinder sites are calculated at the ranging inertial frame location within the USGS cartographic network by applying the appropriate offsets [*Golombek et al.*, this issue]. The target ellipse values are averages of points evaluated along the radar tracks within the USGS network. The radar results at the Pathfinder site are an average of the ranges from the six radar resolution cells containing the Pathfinder landing site. DTM (Digital Terrain Model) from *U.S. Geological Survey* [1993]. Radar from *Haldemann et al.*[1997]. Tracking solution from *Folkner et al.* [1997].

Table 2. Atmospheric Conditions

	Viking Lander 1		Pathfinder Design		Pathfinder Ares Vallis	
	h = 50 km	Surface	h = 50 km	Surface	h = 50 km	Surface
Density (kg/m^3)	1.23×10^{-4}	2.0×10^{-2}	6.6×10^{-5}	2.0×10^{-2}	1.19×10^{-4}	1.74×10^{-2}
Pressure (mbar)	3.45×10^{-2}	6.996	1.722×10^{-2}	6.996	3.68×10^{-2}	6.70
Temperature (K)	147.5	188	137	185.25	163	201±1
Surface Wind (m/s)	--	5 - 10	--	5 - 10	--	5 - 10

Table 3 Site Characteristics

	Landing Site[1] Predictions	Pathfinder Observations
Crater coverage	1.2% of ellipse	3 craters visible, 40% probability these would be visible.
Knob coverage and slopes	0.7% of ellipse Small hills: 10°-25° Large hills: >20°	4 knobs visible, 10% probability these would be visible. Twin Peaks: 14°-27° Far, Southeast, and North Knobs: >30°
Local slopes[2]	3.5 cm delay-Doppler radar: 4.8°±1.3° 3.5 cm CW radar: 6.4°±0.6° 12.6 cm radar: 5°-7°	Preliminary stereogrammetric measurements about 4°
Radar Properties	3.5 cm delay-Doppler normal reflectivity[3]: 0.06±0.02 3.5 cm CW quasi-specular cross-section[3]: 0.045 3.5 cm CW diffuse cross-section: 0.055 12.6 cm: 0.07-0.14	Quasi-specular cross-section: 0.05 (estimate from soil density and area, and rms slope) Diffuse cross-section: 0.07 (estimate from rock abundance, reflectivity, and directivity)
Thermal Inertia, I[4]	Bulk I=**10.4** (9.6-12.9) Fine component I=**8.7** (8.2±0.4) IRTM rock coverage effective I=30	Assuming bulk I=10.4 and rock abundance, implies fine component I=8.4 Rocks in 3-6 m annulus effective I=40
Rock Abundance (% area)	From IRTM: **18 %** (average: 20.4±2.1%, range: 18-25%) From rock size-frequency distribution models: rocks >0.5 m high: 0.7-3.0%	In 3-6 m annulus around lander: average: 16%, range: 10-25% rocks > 0.5 m high: <1%[5]
Color	Albedo: **0.24** (0.19-0.24) Red reflectivity: 0.17-0.18 Violet reflectivity: 0.06-0.07 Red/violet ratio: 2.4±0.3	Abundant dark gray rocks, with less dust and/or weathering than the Viking sites.

See Golombek et al. [1997a] for sources of data for Landing Site Predictions.

[1] Boldface values in this column refer to the pixel containing lander, other values are averages for the whole landing ellipse (100 km by 200 km).

[2] Slopes are reported as a root mean square (rms) angle from horizontal for a sampling of slopes with lengths less than 10 m.

[3] For small rms slopes, normal reflectivity and quasi-specular cross-section are nearly equal.

[4] The units for thermal inertia, I, are 10^{-3} cal cm^{-2} $s^{-1/2}$ K^{-1}.

[5] This is the far-field number, see text.

FIGURE CAPTIONS

Figure 1. Portion of the Mars Pathfinder landing site (top) and Ephrata Fan (bottom). The Ephrata Fan surface was suggested to be analogous to what we expected to find at the Pathfinder landing site prior to landing [*Golombek et al.*, 1997a]. The portion of the Pathfinder landing site is looking due south and covers 10° in azimuth by 5° in elevation (from Super Panorama); largest foreground rocks are 20-50 cm across. Picture of the proximal, rocky portion of the Ephrata Fan looking southeast (courtesy of Vic Baker, University of Arizona), where late stage drainage has been less important. Note dirt road in background for scale; foreground rocks are roughly 30 cm across.

Figure 2. Cumulative fraction of area covered by rocks versus diameter at the Pathfinder landing site, the Viking landing sites and models developed to predict the area covered by large rocks prior to landing by *Golombek and Rapp* [1997]. The Viking 1 and 2 rock distributions are from *Moore and Keller* [1990, 1991], with outcrops at Viking 1 not included. Pathfinder data (black dots) are from an annulus of 3-6 m around the lander. The far field data are estimates made for rocks greater than 1 m and 2 m diameter as described in the text. Model curves are for 5, 10 and 20% total rock coverage as described in *Golombek and Rapp* [1997]. Data show that the cumulative area covered by rocks greater than 1 m diameter is less than 1% at the Pathfinder landing site, consistent with model predictions.

Figure 3. Cumulative fraction of area covered by rocks versus rock height at the Pathfinder landing site, the Viking landing sites and models developed to predict the area covered by large rocks prior to landing by *Golombek and Rapp* [1997]. The Viking 1 and 2 rock distributions are from *Moore and Keller* [1990, 1991], with outcrops at Viking 1 not included. Pathfinder data (black dots) are from an annulus of 3-6 m around the lander. The far field data are estimates made for rocks greater than 1 m and 2 m diameter as described in the text. Model curves are for 5, 10 and 20% total rock coverage as described in *Golombek and Rapp* [1997]. Data show that the cumulative area covered by rocks greater than 0.5 m high is less than 1% at the Pathfinder landing site, consistent with model predictions.

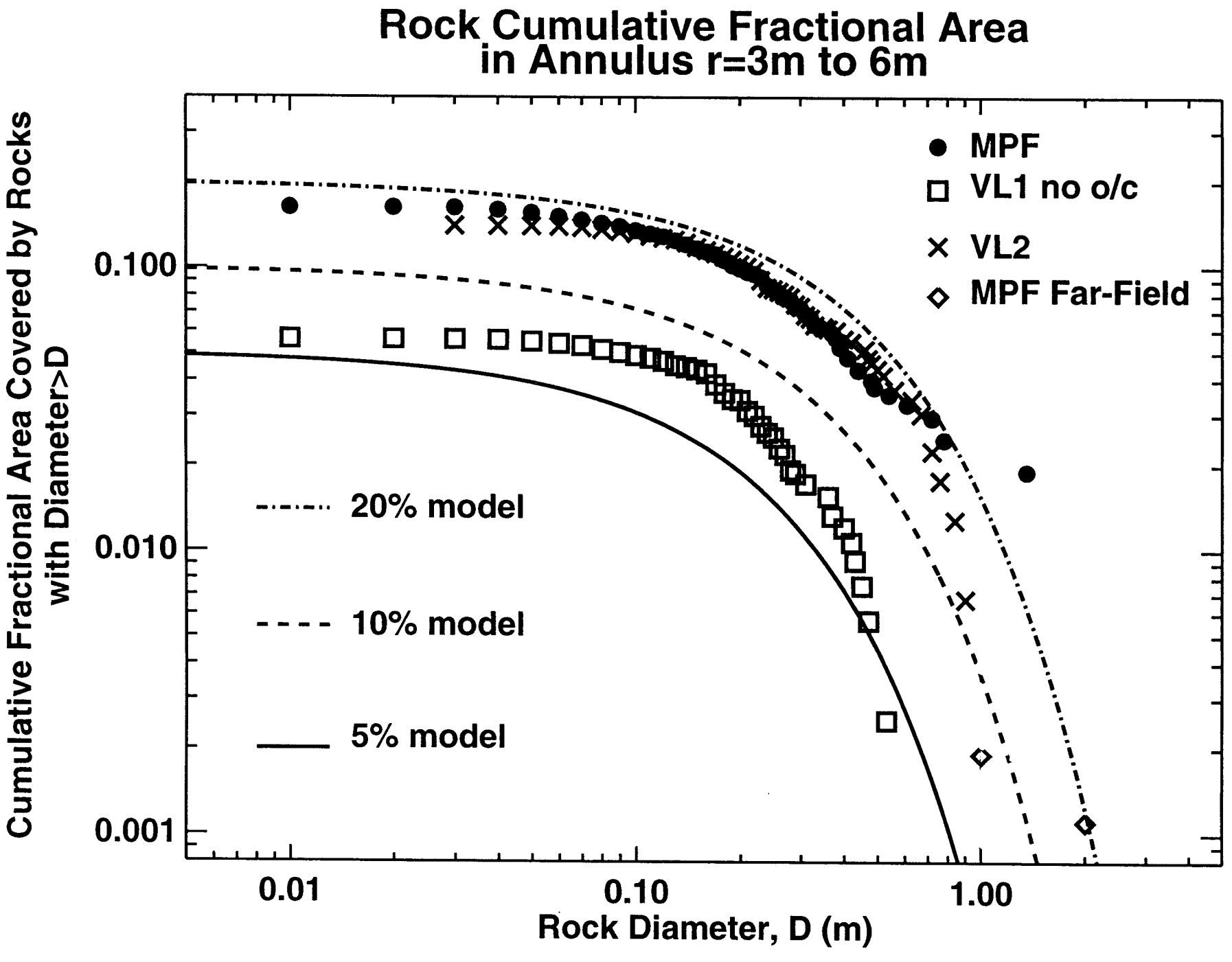
Rock Cumulative Fractional Area
in Annulus r=3m to 6m
Cumulative Fractional Area Covered by Rocks
with Diameter>D
0.100
0.010
0.001
0.01
0.10
1.00
Rock Diameter, D (m)
MPF
VL1 no o/c
VL2
MPF Far-Field
20% model
10% model
5% model

Figure 2

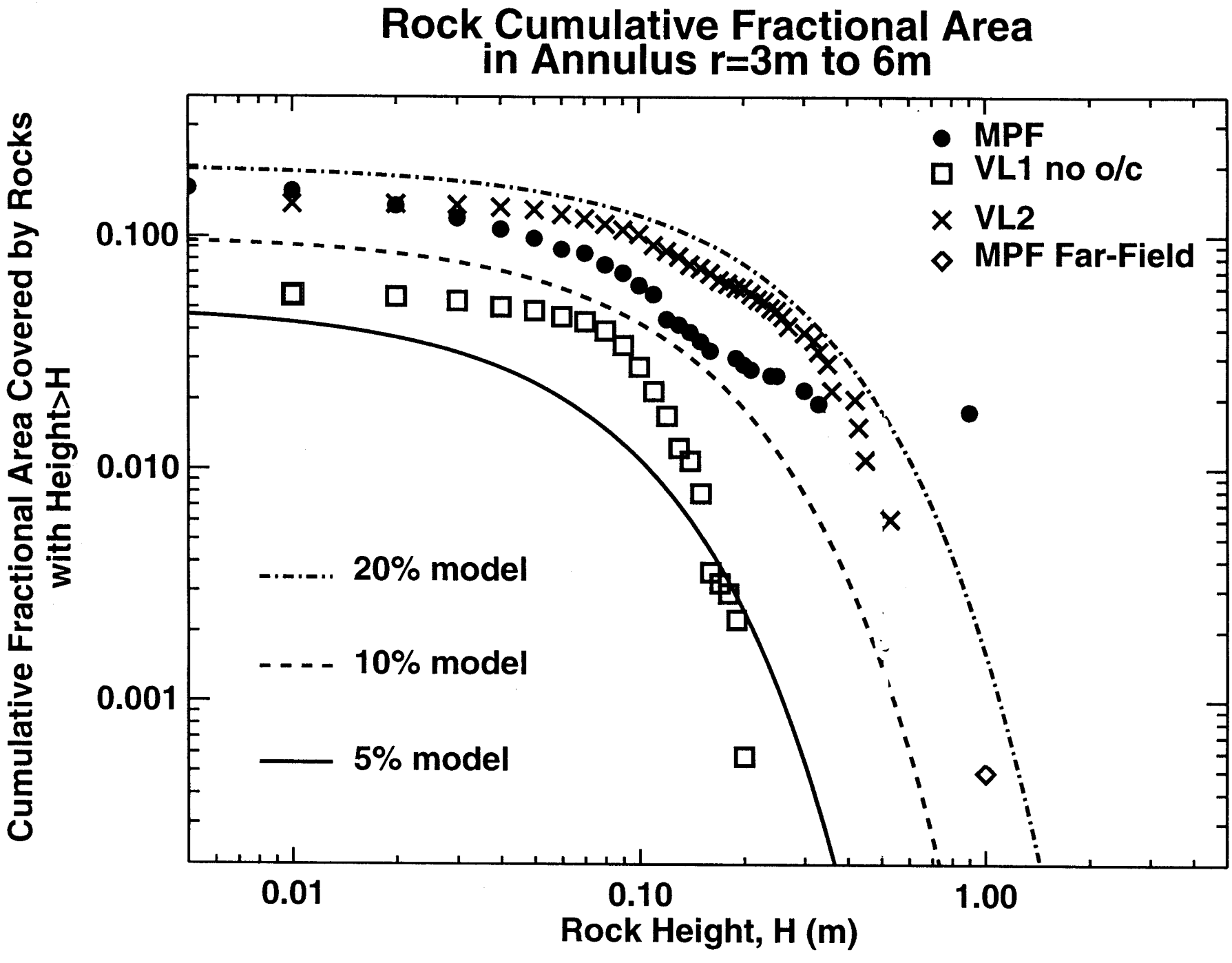
Rock Cumulative Fractional Area
in Annulus r=3m to 6m
Cumulative Fractional Area Covered by Rocks with Height>H
0.100
0.010
0.001
0.01
0.10
1.00
Rock Height, H (m)
MPF
VL1 no o/c
VL2
MPF Far-Field
20% model
10% model
5% model

Figure 3